Check for updates

ADVANCED MATERIALS
www.advmat.de

Fibrous Zr-MOF Nanozyme Aerogels with Macro-Nanoporous Structure for Enhanced Catalytic Hydrolysis of Organophosphate Toxins

Kaikai Ma, Yuk Ha Cheung, Kent O. Kirlikovali, Haomiao Xie, Karam B. Idrees, Xiaoliang Wang, Timur Islamoglu, John H. Xin, and Omar K. Farha**

Metal–organic frameworks (MOFs) with Lewis acid catalytic sites, such as zirconium-based MOFs (Zr-MOFs), comprise a growing class of phosphatase-like nanozymes that can degrade toxic organophosphate pesticides and nerve agents. Rationally engineering and shaping MOFs from as-synthesized powders into hierarchically porous monoliths is essential for their use in emerging applications, such as filters for air and water purification and personal protection gear. However, several challenges still limit the production of practical MOF composites, including the need for sophisticated reaction conditions, low MOF catalyst loadings in the resulting composites, and poor accessibility to MOF-based active sites. To overcome these limitations, a rapid synthesis method is developed to introduce Zr-MOF nanozyme coating into cellulose nanofibers, resulting in the formation of processable monolithic aerogel composites with high MOF loadings. These composites contain Zr-MOF nanozymes embedded in the structure, and hierarchical macro-micro porosity enables excellent accessibility to catalytic active sites. This multifaceted rational design strategy, including the selection of a MOF with many catalytic sites, fine-tuning the coating morphology, and the fabrication of a hierarchically structured monolithic aerogel, renders synergistic effects toward the efficient continuous hydrolytic detoxification of organophosphorus-based nerve agent simulants and pesticides from contaminated water.

1. Introduction

Nanozymes comprise a class of burgeoning nanomaterials with enzyme-like catalytic properties,[1–6] and the development of nanozymes with processability and recyclability is essential for their implementation in practical applications, including pathogen elimination,[7] diagnostics,[8–10] therapy,[11–13] and environmental remediation.[14,15] Metal–organic frameworks (MOFs) constitute an attractive class of porous crystalline materials constructed from highly ordered, extended networks of inorganic nodes and organic linkers.[16–26] Due to their significant tunability and structural diversity, MOFs have been developed as efficient heterogeneous nanozyme catalysts for biomolecule hydrolysis, as well as the detoxification of harmful organophosphorus pesticides and nerve agents.[27–34] The initial construction of MOF nanozyme catalysts for the degradation of organophosphorus toxins drew inspiration from enzymes, which are capable of detoxifying organophosphates, such as phosphotriesterase (PTE), contain Lewis acidic zinc ions pair bridged by a hydroxyl anion as the active catalytic site (**Scheme 1**a).[35] The outstanding structure tunability of MOFs enables the potential design of frameworks that resemble the active sites of enzymes, and our group have demonstrated that Zr-MOFs constructed from Lewis acidic zirconium clusters could sufficiently mimic the dinuclear Zn-based active site in these enzymes for efficient organophosphates catalytic hydrolysis (Scheme 1b–c).[34]

Despite this promising performance, the implementation of MOF nanozyme catalysts in practical applications, such as in filters in continuous catalysis beds or in protective equipment, has been hindered due to technical challenges arising from the poor processability of as-synthesized MOF powders. Shaping MOF powders into processable monoliths or composites is a critical step toward overcoming these limitations.[36–60] One strategy to access pure MOF monoliths involves the shaping of MOFs into monolithic aerogels, which are low density composites with hierarchically porous structures that result in the formation of efficient chemical diffusion pathways.[44,45]

K. Ma, K. O. Kirlikovali, H. Xie, K. B. Idrees, X. Wang, T. Islamoglu, O. K. Farha
Department of Chemistry and International Institute for Nanotechnology
Northwestern University
2145 Sheridan Road, Evanston, IL 60208, USA
E-mail: kaikai.ma@northwestern.edu; o-farha@northwestern.edu

K. Ma, Y. H. Cheung, J. H. Xin
School of Fashion and Textiles
The Hong Kong Polytechnic University
Hung Hom, Hong Kong, SAR China

O. K. Farha
Department of Chemical and Biological Engineering
Northwestern University
2145 Sheridan Road, Evanston, IL 60208, USA

The ORCID identification number(s) for the author(s) of this article can be found under https://doi.org/10.1002/adma.202300951

© 2023 The Authors. Advanced Materials published by Wiley-VCH GmbH. This is an open access article under the terms of the Creative Commons Attribution License, which permits use, distribution and reproduction in any medium, provided the original work is properly cited.

DOI: 10.1002/adma.202300951

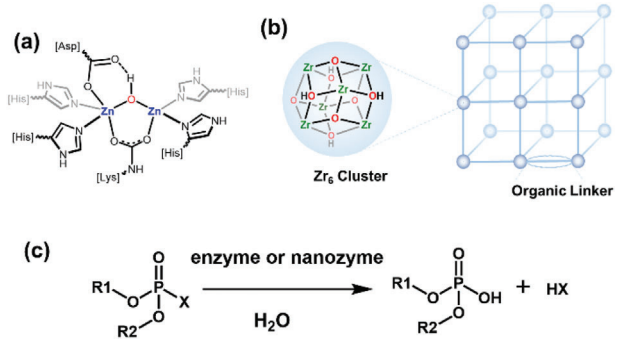

Scheme 1. Mimicking the Lewis acidic zinc active sites in PTE with Lewis acidic zirconium-based MOFs. a) Diagram of the Lewis acidic zinc pair active site in PTE. b) Simplified representation of a Zr-MOF showing Lewis acidic zirconium active site on the node. c) General reaction scheme for the catalytic hydrolysis of organophosphorus substrates with an enzyme or nanozyme catalyst.

However, the inherent fragility of pure MOF aerogel monoliths has restricted their development.[45] In an effort to overcome these limitations, researchers combined processable polymeric substrates with MOFs to afford MOF-polymer composites, such as fibers, foams, and films, that feature enhanced practicality and functionality.[36–54] However, several challenges limit the practical implementation of MOF-based composites, including the need for sophisticated production equipment, insufficient MOF loadings in the composites, and poor accessibility to MOF-based active sites.[35,46,47] Considering these drawbacks, the facile and efficient synthesis of flexible and processable monolithic MOF composite materials with good functional MOF accessibility would enable the use of MOF aerogel catalysts in practical settings, especially for realistic catalytic detoxification applications, as these catalysts could be shaped into a desired form for each unique setting.[61–64]

In this work, we developed a rapid, high-efficiency coating method to produce zirconium-based MOF (Zr-MOF) nanozyme monolithic composites using fibrous bacterial cellulose (BC) network as a low cost and easily accessible supporting substrate (**Figure 1**a,b; Figures S1 and S2, Supporting Information). Introducing a highly concentrated solution of MOF precursors into the BC substrate by exchange enables the formation of a crystalline, porous, and interconnected MOF coating after heating the reaction mixture for a few hours. Activation of the wet MOF-containing gel using supercritical CO_2 removes the guest solvent molecules from the material and affords a low weight aerogel composite with controllable high MOF mass loading (up to 90%), hierarchical macro-micro porosity, and good processability (Figure 1 and Figure S1, Supporting Information). The rational combination of a highly active Zr-MOF nanozyme catalyst with flexible and macroporous cellulose nanofiber substrates, which endow the hierarchical structure with better accessibility to MOF-based catalytic sites, generates a material capable of rapidly detoxifying harmful organophosphorus chemicals in both batch and continuous reactions under practical conditions (Figure 1c).

2. Results and Discussion

We chose the Zr-MOF MOF-808 as the model MOF nanozyme for the composite synthesis because the relatively low node connectivity of the Zr_6-based nodes (6-connected) results in a large number of Lewis acidic active sites available for catalysis to occur.[65] To synthesize the MOF nanozyme composite, we first created a solution containing the MOF-808 precursors ($ZrOCl_2 \cdot 8H_2O$ as the metal source and trimesic acid as the ligand) at 6-, 8-, and 10-fold increased concentrations (0.066–0.11 M based on ligand) relative to the concentration employed to synthesize MOF-808 powder by Yaghi (0.011 M based on ligand).[66] Next, we introduced the natural bacterial cellulose as the nanofiber substrate into the reaction mixture, and the MOF-808 precursor solution exchanged into the BC network over the course of 1 h at 100 °C to trigger the formation of the MOF-808 coating onto cellulose nanofiber. After washing and exchanging solvents used for synthesis with ethanol, we obtained MOF-coated cellulose nanofiber composites as wet gels, which could then be activated using supercritical CO_2 ($scCO_2$) to yield the MOF nanozyme-containing monolithic aerogel composite (Figure 1 and Figures S3–S5, Supporting Information). Powder X-ray diffraction (PXRD) analysis of the composites reveals diagnostic MOF-808 peaks, confirming the successful integration of MOF-808 into these materials (**Figure 2**a). Notably, the reaction to generate this MOF coating proceeds significantly faster than most traditional methods used to synthesis MOF-based coatings and composites (typically 2–3 days).[66] In fact, these prolonged reaction times used in original MOF-808 powder synthesis could damage the BC matrix and form a slurry, so the fast reaction developed for MOF nanozyme aerogel composites is essential to maintain the integrity of fibrous cellulose substrate. In this system, a combination of the hydroxyl-rich surfaces of the cellulose nanofibers potentially inducing localized MOF formation and a high concentration of MOF precursors likely leads to the rapid nucleation and growth of the MOF-808 coating on the cellulose fiber substrate. When we decreased the concentration of the MOF precursor solution below 0.044 M, we did not observe the formation of any MOF-808 coating on the BC nanofibers after the same reaction time of 1 h.

The activated fibrous MOF-808 nanozyme aerogel composites, which were synthesized from the reactions with 0.066, 0.088, and 0.11 M MOF-808 precursor (based on ligand), are denoted as FMOF-808-NA1, FMOF-808-NA2, and FMOF-808-NA3, respectively (Figures S3–S5, Supporting Information). Inductively coupled plasma-optical emission spectrometry (ICP-OES) analysis of the three composites revealed MOF-808 mass loadings of 80, 84, and 89 wt%, respectively. It is notable that the MOF-808 volumetric loading in the three composites is 40, 55, 68 mg cm^{-3}, respectively, which shows good correlation with the concentration of each precursor solution and indicates that the MOF loading is controllable by adjusting the precursor concentration (Table S1 and Figure S6, Supporting Information). N_2 sorption isotherms obtained at 77 K for the composites illustrate that the porosity of these materials dramatically improves upon the introduction of MOF-808 (Figure 2b). For instance, the Brunauer–Emmett–Teller (BET) surface area (S_{BET}) of pure bacterial cellulose is only 80 $m^2\ g^{-1}$, while the S_{BET} values are 1400, 1430, and 1520 $m^2\ g^{-1}$ for FMOF-808-NA1, FMOF-808-NA2, and FMOF-808-NA3, respectively. The normalized BET surface areas of the MOF-808 component in the composites ranges from 1700 to 1750 $m^2\ g^{-1}$ (Table S1, Supporting Information), which is close to values of 1500–2000 $m^2\ g^{-1}$ reported for nanosized MOF-808

© 2023 The Authors. Advanced Materials published by Wiley-VCH GmbH

Downloaded for personal academic use. All rights reserved. https://papernode.online/

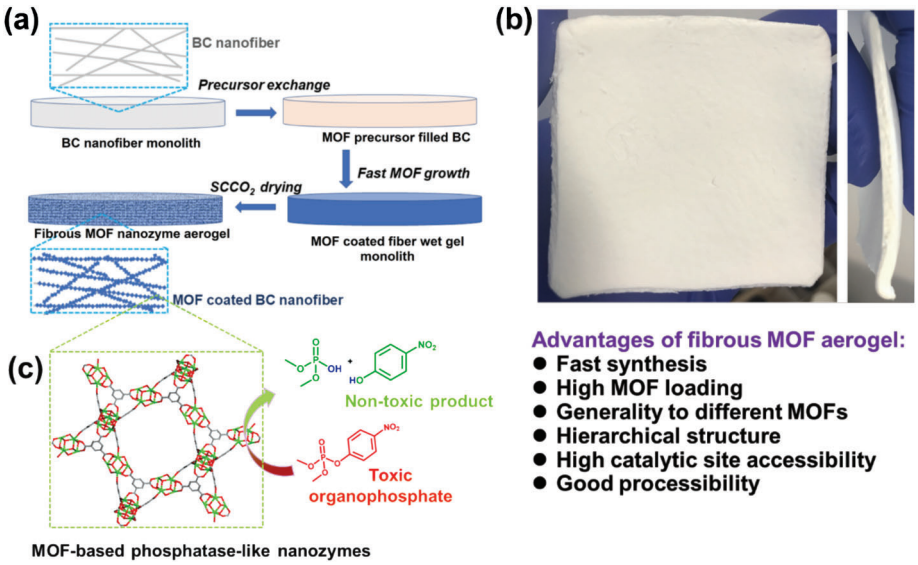

Figure 1. a) Schematic illustration of fast growth method to fibrous Zr-MOF nanozyme aerogel, b) representative fibrous MOF-808 nanozyme aerogel composite sample (5 cm × 5 cm × 0.3 cm), c) illustration of MOF based phosphatase-like nanozyme for toxic organophosphate degradation by catalytic hydrolysis.

nanoparticles.[22,66] In addition, we observed the characteristic MOF-808 intraparticle pore of about 1.7 nm in diameter in the composites, suggesting these pores remain accessible in the composite with diameter about 1.7 nm was detected (Figure S7, Supporting Information). Scanning electron microscope (SEM) images obtained for the composites illustrate both their macroporous 3D morphology and the even distribution of the MOF nanoparticle coating on fiber surface to form a core-shell structure (Figure 2c–f; Figure S8–S11, Supporting Information). The diameter of BC without the MOF coating is about 50 nm, while the fiber diameter increases to between 100 and 150 nm for FMOF-808-NA1, FMOF-808-NA2, and FMOF-808-NA3. In addition, we clearly observe macropores on the order of several microns in the composites (Figure 2c–f). This hierarchical macro-micro porous structure should enhance diffusion of the reagents to the active sites in the composite and enhance catalytic performance (vide infra). Element analysis by energy-dispersive X-ray spectroscopy (EDX) mapping of FMOF-808-NA1 to -A3 samples shows a uniform distribution of Zr in the samples, indicating a homogenous distribution of the MOF-808 coating throughout the aerogel composites (Figure S12–S14, Supporting Information). X-ray photoelectron spectroscopy (XPS) analysis of the aerogel samples further indicates the presence of MOF-808 based on the observation of characteristic zirconium elements in the composites and the binding energy shift of oxygen on MOF-808 after deposition on BC fiber implies the possible existence of direct interactions, such as coordination, between BC surface and MOFs layer (Figure S15, Supporting Information). The presence of MOF-808 on composite is also evidenced by the characteristic peak of carbonate group from MOF-808 in FTIR study (Figure S16, Supporting Information). Overall, these comprehensive studies reveal the successful introduction of MOF-808 into composite.

In comparison to the hierarchically porous MOF-808 nanozyme aerogels obtained from $scCO_2$ activation of the MOF-808-coated cellulose wet gels, drying the wet gel composite samples directly in air affords a composite denoted as FMOF-808 xerogel-1, which features a condensed morphology of stacked fibers and a nonhierarchical structure without any obvious macropores (**Figure 3**a and Figure S17, Supporting Information). Comparison of the SEM images obtained for the macroporous 3-D aerogel (FMOF-808-NA1) and less macroporous xerogel sample (FMOF-808 xerogel-1) further highlights the significant morphological differences between these two samples (Figure S18, Supporting Information). Although PXRD analysis and N_2 sorption isotherms indicate that MOF-808 is still intact in FMOF-808 xerogel-1, increasing uptake in the high relative pressure region of the N_2 sorption isotherm suggests interparticle aggregation of MOF-coated fibers (Figure 3b and Figure S18, Supporting Information).[44] Combined, these results illustrate the importance of both the 3D nanofibrous BC scaffold and the relatively gentle $scCO_2$ activation strategy in the formation of the hierarchically porous MOF-coated fibers in these aerogel composites. Notably, this fast-coating synthesis method can be extended to the incorporation of different Zr-MOFs into the BC matrix. For example, we introduced fibrous UiO-66, UiO-66-NH_2, and Zr-BTB nanozyme aerogels, denoted as FUiO-66-NA1, FUiO-66-NH_2-NA1, and FZr-BTB-NA1 (Figures S19–S33, Supporting Information), respectively, using an analogous method to that described for FMOF-808-NA1. We verified the crystallinity, porosity, and hierarchical structure of these sponge-like composites using PXRD, N_2 sorption isotherms, and SEM imaging, respectively (Figures S23–S33, Supporting Information), illustrating the generality of this fast gelation method and confirming that we could introduce different functionalities into the composites simply by changing precursors.

For these monolithic MOF aerogels to be employed in real-world applications, such as air- or water- cleaning filters, excellent mechanical stability is a critical prerequisite. For instance,

© 2023 The Authors. Advanced Materials published by Wiley-VCH GmbH

Downloaded for personal academic use. All rights reserved. https://papernode.online/

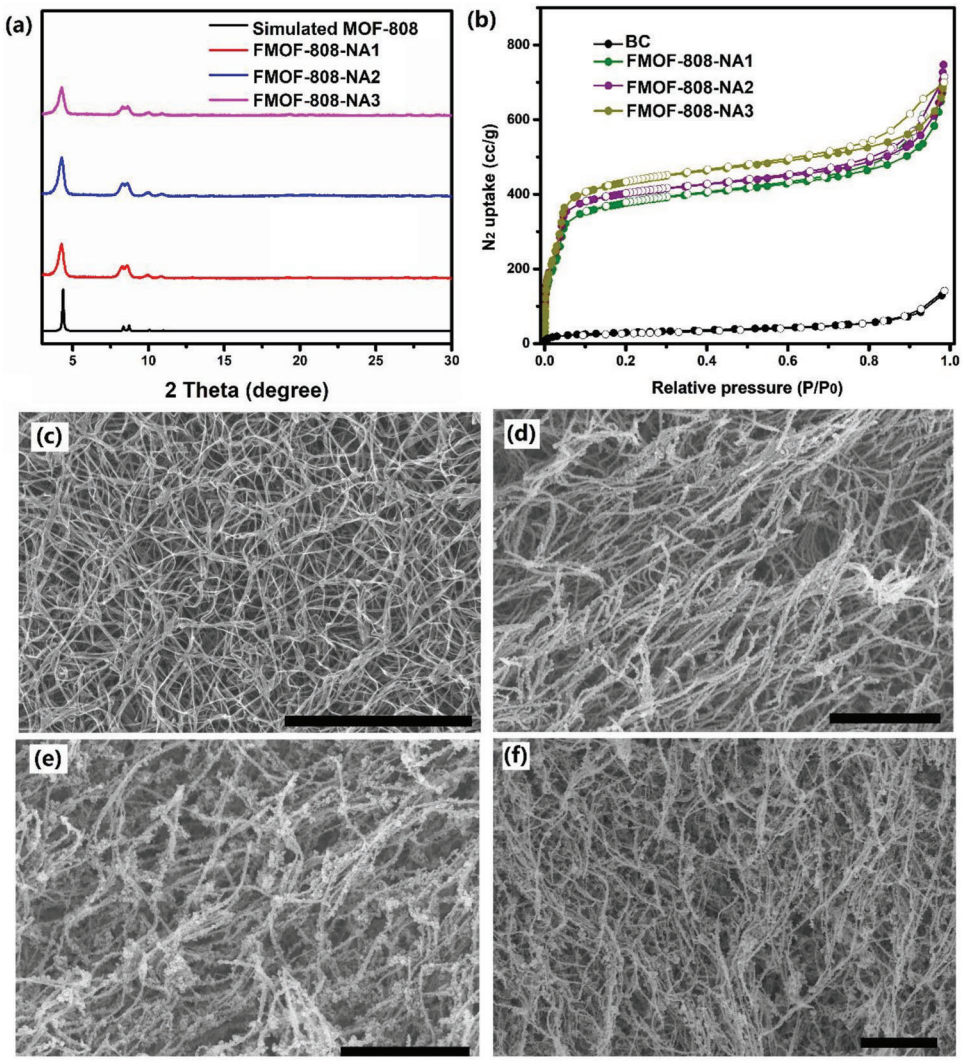

Figure 2. Characterization of fibrous MOF-808 nanozyme aerogel composites, FMOF-808-NAx (x = 1–3). a) PXRD patterns; b) nitrogen sorption isotherms; SEM images of c) BC, d) FMOF-808-NA1, e) FMOF-808-NA2, and f) FMOF-808-NA3. Scale bars are 5 μm.

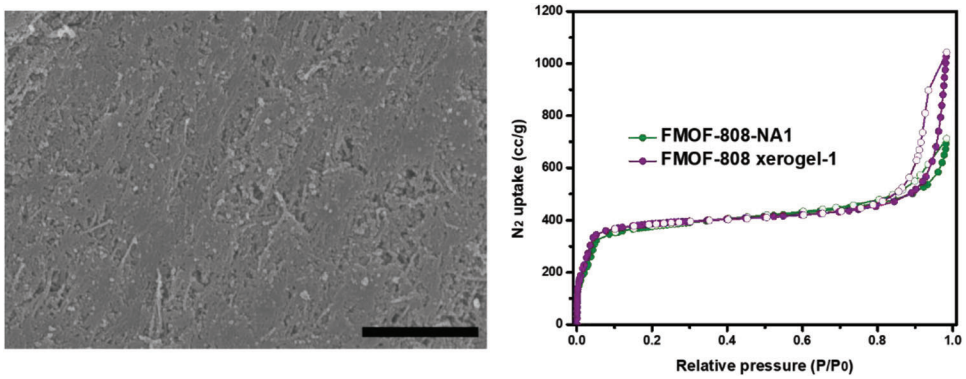

Figure 3. The effect of activation methods on the sample morphologies and porosities. a) SEM image of FMOF-808 xerogel-1 and b) N_2 sorption isotherm comparison between samples from different activation methods. Scale bar is 5 μm.

© 2023 The Authors. Advanced Materials published by Wiley-VCH GmbH

Downloaded for personal academic use. All rights reserved. https://papernode.online/

crushing the monolith may lead to leaching of the MOF particles that would ultimately degrade the functionality and work capacity of these composites. First, we tested the mechanical stability of the FMOF-808-NA1, FMOF-808-NA2, and FMOF-808-NA3 by stirring aqueous suspensions containing these composites at 200 rpm for 24 h. There is no observable leaching of particles into solution during stirring, and ICP-OES testing reveals the same MOF mass loading after stirring as before, indicating the MOF coating is stable under this agitation challenge. The flexibility of the BC matrix could account for the maintained integrity by not only counteracting the shear force during agitation, but also by affording favorable confinement effects for the 3D BC fibrous matrix. These composites are bendable and rollable, making them processable for use in practical applications, such as in mask fillers or filters (Figure S34, Supporting Information). We also quantitatively measured the breaking strength of samples (5 cm × 1 cm × 0.3 cm) by tensile testing according to a grab test method (ASTM D5034-21: Standard test method for breaking strength and elongation of textile fabrics). The bacterial cellulose aerogel without MOF coating shows a tensile strength of 15 N, whereas the tensile strength values for FMOF-808-NA1, FMOF-808-NA2, and FMOF-808-NA3 are 14, 9, and 7 N, respectively (Figure S35, Supporting Information). In other words, the tensile strength decreases as the MOF loading in the composite increases, which is likely due to the acidic degradation of the cellulose polymer backbone that results from contact with the precursor solution that contains organic acids and the zirconium oxychloride salt during synthesis.[67] To understand how the tensile strength values of FMOF-808-NA1 to -A3 compare to those of commercialized porous polymer materials, we tested the tensile strength of a commercial melamine sponge of the same size and using the same method. The tensile strength of the sponge is 5 N, which is similar to value of FMOF-808-NA3, suggesting that the prepared fibrous MOF-808 nanozyme aerogels are capable of the processing and handling techniques used in practical applications. Moreover, the excellent flexibility of these monolithic MOF aerogel composites enables processing them using techniques like tailoring to a desired shape to fit a filtration catalysis device system (Figure S36, Supporting Information).

After synthesizing the fibrous MOF nanozyme aerogel composites, which exhibit hierarchical porous structures and high MOF loadings, we explored the activity of these materials as hydrolytic nanozyme catalysts toward the degradation of the organophosphorus nerve agent simulant dimethyl-4-nitrophenyl phosphate (DMNP) in 0.4 M *N*-ethylmorpholine solution (**Figure 4**a).[46] We monitored the catalytic conversion of DMNP to the nontoxic product dimethyl phosphate (DMP) using ^{31}P nuclear magnetic resonance (NMR) spectroscopy (Figure 4b and Figure S37, Supporting Information). FUiO-66-NA1 achieves about 20% conversion after 10 min, while FUiO-66-NH_2-NA1 and FZr-BTB-NA1 both hydrolyze about 60% of the DMNP substrate after 10 min. In comparison, the FMOF-808-NA1, FMOF-808-NA2, and FMOF-808-NA3 nanozyme samples achieve quantitative DMNP conversion within 10 min under analogous conditions. Through comparison studies with other fibrous Zr-MOF aerogel composites, we ascribe the excellent catalytic activity of the nanozyme catalysts FMOF-808-NA1, FMOF-808-NA2, and FMOF-808-NA3 to the following factors: 1) the lower connectivity Zr node (6-connected) in the MOF-808 structure offers accessible active metal sites, and 2) the large pore size (1.7 nm diameter) enables substrate and product diffusion to and from the catalytic active sites.[23,65] To prove the presence of open metal sites in the MOF nanozyme aerogels, we collected ^{1}H NMR data for a digested MOF nanozyme aerogel sample (FMOF-808-NA1). We found that for this activated composite sample, MOF-808 has 2 formates per node (Figure S38a, Supporting Information), which corresponds to four accessible zirconium metal sites (i.e., four Lewis acidic catalytic sites) per node. Importantly, the formate modulators on the MOF-808 nodes can be easily removed under basic reaction conditions. For instance, after 2 min treatment with basic reaction media, only 0.4 formates per node remain (i.e., roughly 5.6 zirconium sites per node are open; Figure S38b, Supporting Information), which indicates that most of the Lewis acidic open zirconium sites on the MOF nodes are accessible during the reaction. The high catalytic efficiency of the MOF-808 nanozymes in these monolithic aerogel composites is consistent with previous studies that performed similar hydrolysis reactions using powdered MOF-808 catalysts.[40,65] While Zr-BTB is also constructed with a 6-connected Zr node, this MOF is assembled by 2D metal–organic layers and features a pore diameter of only 1.1 nm, which reduces the accessibility to the catalytic Zr nodes between layers (Figure S29, Supporting Information).[22] These experiments illustrate how the rational choice of an appropriate Zr-MOF for the active nanozyme coating, which contains many Zr node-based Lewis-acid catalytic sites and relatively large pores for improved diffusion, can dramatically improve catalytic activity of the resulting aerogel composites.[40]

After determining that FMOF-808-NA1 to -NA3 exhibit the best performance among this series of Zr-MOF nano aerogel composites, we further explored the kinetics of DMNP hydrolysis with these samples in basic aqueous solutions to elucidate any differences in reactivity. Surprisingly, all three materials exhibit quantitative DMNP conversion after only 2 min, which indicates a half-life for DMNP hydrolysis of about 1 min (Figure 4c and Figure S39, Supporting Information). In a control experiment, the cellulose nanofiber matrix in the absence of MOF-808 did not show significant conversion of DMNP, suggesting the catalytic activity observed is solely due to the MOF-808 nanozyme coatings. In fact, the half-life values obtained for FMOF-808-NA1, -NA2, and -NA3 are similar to that of the free MOF-808 nanoparticles suspended in a basic aqueous solution,[23,65] indicating that the aerogel structure enables excellent accessibility to the MOF-808-based active sites in the aerogel composite. In our previous studies, we found that the catalytic activity of MOF composites decreases as the MOF loading increases due to a combination of increasing particle aggregation and decreasing external surface area that hinders substrate diffusion (Table S2, Supporting Information).[46,47] For example, in our previous work, we studied a relatively less macroporous composite with a MOF-808 coating on a textile fiber, and the half-life for DMNP hydrolysis increased by a factor of six when the MOF weight % in the coating increased from 6.5% to 22% (Table S2, Supporting Information).[46] Although the composite sample from that study with 12% MOF loading and the aerogel composite sample in this study with 90% MOF loading, FMOF-808-NA1-3, both exhibit half-lives for DMNP hydrolysis of 1 min, the weight of FMOF-808-NA3 is 7.5 times lower than that of the composite from the previous study (Table S2, Supporting Information).[46]

© 2023 The Authors. Advanced Materials published by Wiley-VCH GmbH

Downloaded for personal academic use. All rights reserved. https://papernode.online/

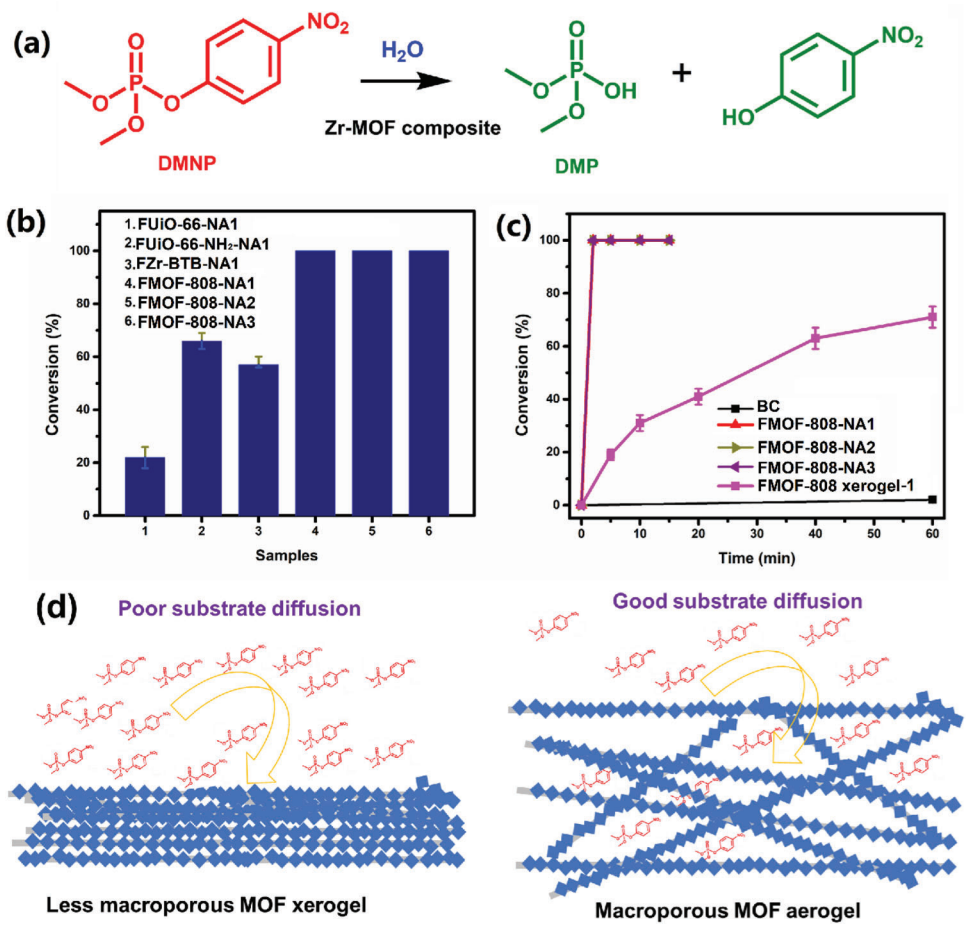

Figure 4. a) Catalytic hydrolysis reaction of DMNP by fibrous Zr-MOF nanozyme aerogel catalysts. b) DMNP conversion after 10 min with different fibrous Zr-MOF nanozyme aerogel catalysts. c) DMNP conversion kinetics with different fibrous MOF-808 nanozyme aerogel catalysts. Conditions: 1.5 µmol Zr-MOF in composite (corresponding to 6 mol % catalyst) and 25 µmol DMNP used in catalysis reactions. d) Illustration of the differences in diffusion between the less macroporous MOF nanozyme xerogel (left) and the microporous MOF nanozyme aerogel (right).

In other words, the fibrous aerogel nanozymes could improve the specific working capacity (normalized with the same composite weight) by a factor of 7.5. More broadly, these aerogel nanozyme composites are lightweight and efficient catalytic materials with high MOF loadings and relatively high working capacities, which suggests they could be highly valuable materials in a wide variety of applications.

To further compare the catalytic activities of FMOF-808-NA1-3 with those of previously reported MOF nanozyme composites, we introduced the concept of turnover factor (TOF), which evaluates the catalytic performance of these materials normalized to the composite weight (Figure S40 and Table S2, Supporting Information) since the development of high-performance, lightweight catalytic nanozyme composites is an important consideration for their potential implementation in practical applications. We found that FMOF-808-NAx ($x = 1, 2, 3$) shows the best TOF normalized by composite weight relative to those of similar nanozyme composites, and these TOF values are one order of magnitude higher than almost every other similar composite reported. Importantly, TOFs normalized by composite weight for FMOF-808-NAx ($x = 1–3$) increase as the MOF loading increases, while TOFs for previously reported MOF-808-PET samples decrease as the loading increases (samples 1–3 and samples 11–13 in Figure S40; Table S2, Supporting Information). Not only are the catalytic activities observed for these BC-supported MOF-808 aerogel monolith samples among the highest values reported for MOF composite-based catalysts, but the synthesis method reported in this study is more rapid and efficient, and it affords composites with higher MOF loadings (up to about 90%) and enhanced work capacities (Table S2, Supporting Information).

To confirm that the macropores in the fibrous MOF-808 nanozyme aerogels benefit catalysis by promoting diffusion of the organophosphorus substrates to the MOF-based catalytic active sites, we performed DMNP hydrolysis reactions using the less macroporous MOF-808-xerogel-1 as the catalyst (vide supra). The xerogel sample exhibits a half-life for DMNP hydrolysis of 30 min under otherwise analogous conditions (Figure 4c and Figure S41, Supporting Information), indicating that formation of the macroporous aerogel structure affords a nanozyme composite catalyst with a 30-fold increase in catalytic activity. The relatively better catalytic performance of the fibrous MOF-808 aerogel likely originates from the hierarchical pore structure that enhances accessibility of MOF nanozyme catalyst for reagent diffusion, and subsequently, a faster reaction rate (Figure 4d).

© 2023 The Authors. Advanced Materials published by Wiley-VCH GmbH

Downloaded for personal academic use. All rights reserved. https://papernode.online/

Moreover, the aerogel sample outperforms the xerogel sample in a DMNP uptake test from neutral water solution, emphasizing how the macroporous structure of the aerogel samples enables enhanced agent diffusion compared to the relatively less microporous structure in the xerogel sample (Figure S42, Supporting Information). Importantly, the catalytic performance of the FMOF-808-NA1 composites could be fully retained for at least 3 cycles by subjecting them to a simple washing method following catalysis, implying the composite could be reused effectively for multicycle catalysis reactions (Figure S43, Supporting Information). Moreover, after aging the FMOF-808-NA1 sample in air in an open 2-dram glass vial for 3 months, the catalytic performance remained intact and comparable to that of the freshly prepared sample (Figure S43, Supporting Information). Combined, these results indicate that the BC-supported MOF aerogel composites are promising nanozyme materials for the hydrolytic degradation of organophosphorus nerve agent simulants due to their high catalytic efficiency, reusability, and excellent stability. We tested the DMNP elimination with MOF-808-NA1 from real tap water, and catalytic degradation activity is the same as that in DI water, which means the nanozyme filter could be extended to real application fields (Figure S44, Supporting Information).

Given the high catalytic nanozyme activity and good processability of the fibrous MOF nanozyme aerogels, we explored their potential for the continuous detoxification of DMNP solutions to mimic a practical strategy for cleaning water contaminated with toxic organophosphorus compounds (Figure 4). To prepare a MOF plug-flow reactor, we added a piece of FMOF-808-NA1 (1 cm in diameter, 0.1 cm in thickness, 3 mg) into the filter head as the catalytic filler (Figure S45, Supporting Information). We then injected an aqueous solution containing 40 µL (250 µmol) of simulant through the plug-flow reactor at a rate of 0.1 mL min^{-1} using a micropump, and the filtrate was subjected to ^{31}P NMR spectroscopic analysis every 1 mL to determine DMNP conversion (Figure S46, Supporting Information). As shown in Figure 4b, the catalytic hydrolysis reaction achieved total conversion for the first 10 mL and dropped to 92% conversion for the twelfth mL. At this point, we regenerated the nanozyme filter by washing it with 50 mL water and loaded it back into the plug-flow reactor. The regenerated catalyst filter achieved quantitative DMNP conversion for the 13th to 23rd mL of DMNP solution (Figure 4b and Figure S45, Supporting Information), illustrating that the nanozyme catalyst filter can be regenerated in a straightforward manner. Compared powered nanozyme catalyst, the fibrous aerogel composite is more practical for installing and regeneration.[65]

To further increase the application potential of the Zr-MOF-based nanofibrous nanozyme filter, we explored its ability to catalytically hydrolyze dichlorvos (DDVP), which is a widely used organophosphorus-based pesticide, into the nontoxic product DMP (Figures 5c and Figures S46–S49, Supporting Information).[68] First, we probed the performance of FMOF-808-NA1 toward the hydrolysis of DDVP in basic aqueous solutions and observed a half-life for hydrolysis of 1 min, which is comparable to the half-life for DMNP hydrolysis observed under analogous conditions (Figures S48–S49, Supporting Information). This fast degradation kinetics highlight the potential for these fibrous MOF nanozyme aerogel catalysts to be employed in the detoxification of organophosphorus pesticides from contaminated water. Next, we studied the continuous hydrolysis performance of DDVP with FMOF-808-NA1 as the active nanozyme filter using the same protocol previously described for DMNP (**Figure 5**c and Figures S50–S51, Supporting Information). Under these conditions, we observed quantitative conversion of DDVP into the nontoxic product DMP in the first 11 mL, which then slightly decreased to 94% DDVP conversion after the 13th mL. After regeneration of the FMOF-808-NA1 nanozyme catalyst filter by simple washing, we again observed quantitative DDVP conversion for the 14th mL until at least the 25th mL (Figure 5c and Figure S49, Supporting Information). Combined, these results illustrate both the processability and the potential for the freestanding aerogel nanozyme catalyst to be implemented for the continuous catalytic hydrolysis of toxic organophosphate chemicals under practical conditions.

Finally, we demonstrated the successful synthesis of fibrous MOF-808 nanozyme aerogels with inexpensive, commercialized BC nanofiber material, rather than the BC synthesized according to the method described in our work. We found that these nanozyme aerogels made with commercial BC show similar properties and catalytic performance to those of the aerogels made from synthesized BC, proving that this method is extendable to easily accessible commercialized BC fibers (Figure S52, Supporting Information). Importantly, the cost of BC is only about 10% of the cost of the MOF precursors (e.g., the metal salt and organic linker), further emphasizing the economic advantages of employing BC as a substrate to synthesize high-performance fibrous MOF nanozyme aerogels.

3. Conclusion

In this work, we have developed a rapid protocol to synthesize monolithic, hierarchically porous MOF nanozyme aerogel composites that show excellent enzyme-mimetic catalytic activity toward the hydrolysis of organophosphorus nerve agents and pesticides. In addition to high MOF loadings, these monolithic composites also feature high surface areas, low densities, and excellent processabilities, and the flexible BC matrix endows the composites with robust stability against mechanical agitation. The hierarchical porosity formed from a combination of the macroporous cellulose nanofiber aerogel matrix and the microporous Zr-MOF nanozyme affords a solid-state composite with exceptional substrate accessibility to the Zr-MOF-based active sites. We found that the aerogel composites FMOF-808-NA1, -NA2, and -NA3 demonstrate the best performance toward catalytic hydrolysis of the organophosphorus nerve agent simulant DMNP and pesticide DDVP, with half-lives for hydrolysis on the order of 1 min. We then showed that these monolithic aerogel composites could be used in continuous flow settings for large-scale organophosphorus substrate detoxification, and they could be easily regenerated by washing with the composite with water. Overall, the straightforward and versatile synthesis method for these fibrous Zr-MOF nanozyme aerogel composites, combined with their excellent catalytic detoxification and permeation performance, positions them as potential next-generation materials for the effective degradation of toxic nerve agents and pesticides in practical applications.

© 2023 The Authors. Advanced Materials published by Wiley-VCH GmbH

Downloaded for personal academic use. All rights reserved. https://papernode.online/

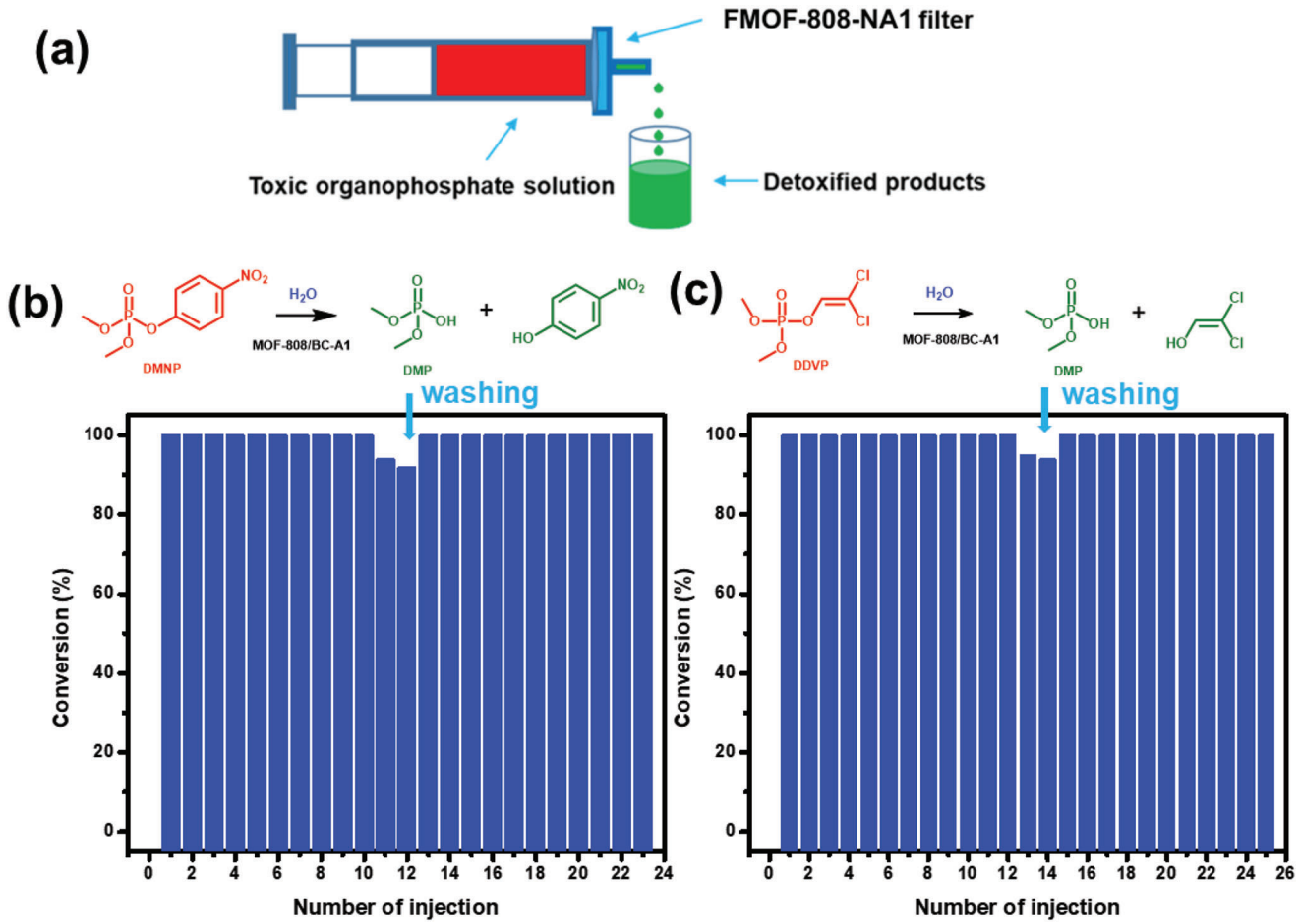

Figure 5. a) Schematic representation of the continuous hydrolysis of toxic organophosphate nerve agent simulant and pesticide using a plug-flow reactor with FMOF-808-NA1 as the nanofibrous nanozyme filter. b,c) Conversion of toxic DMNP and DDVP to nontoxic dimethylphosphate after different injections through the plug flow (1 mL per injection); flow rate 0.1 mL min^{-1}; catalyst was washed with water and re-loaded after 12 and 13 injections, respectively, for these two reactions.

4. Experimental Section

General Procedure for Preparation of Fibrous MOF-808 nanozyme Aerogel Samples: BTC (2.1 g, 10 mmol) and $ZrOCl_2 \cdot 8H_2O$ (9.7 g, 30 mmol) were dissolved in a DMF/formic acid (1/1 v/v) solvent mixture under sonication for 10 min to afford precursor solutions with concentrations from 0.066 to 0.11 M (based on BTC ligand). One piece of round shape BC (90 mm in diameter and 3 mm in thickness) and 50 mL of the above precursor solution were added into a 500 mL Pyrex Schott bottle, and the mixture was ultrasonicated for 1 h for the diffusion of precursors into the BC matrix. The capped vial was heated to 100 °C for 1 h. The wet composite gel was separated with tweezers and washed with 50 mL ethanol (×3) for 2 h each time. The ethanol-exchanged wet gels were activated using supercritical CO_2 using a Tousimis Samdri-931 critical point dryer at a bleed rate of 1.0 mL min^{-1} to afford the aerogel samples FMOF-808-NA1, -A2, and -A3.

Liquid-Phase Catalytic Hydrolysis of DMNP and DDVP: Catalytic hydrolysis of DMNP experiments were carried out at room temperature and monitored by in situ ^{31}P NMR.[47] All activated fibrous Zr-MOF nanozyme composite catalysts were cut into small pieces (1 mm × 1 mm × 1 mm). All fibrous composite samples containing 1.5 µmol MOF were added into a 3-dram vial. DMNP or DDVP (25 µmol) was dissolved in 0.4 M *N*-ethylmorpholine solution (1 mL; 0.05 mL *N*-ethylmorpholine, 0.9 mL DI water/0.1 mL D_2O) and transferred into the vial. The sealed vial was vortexed for 10 s and magnetically stirred at 100 rpm. The simulant solution was filtered using a 200 nm syringe filter and transferred to an NMR tube for collection of ^{31}P NMR spectra. The catalytic activity of pure BC without MOF was also evaluated under identical conditions as a control.

Continuous Catalytic Hydrolysis of DMNP and DDVP with FMOF-808-NA1 Filter: To prepare the MOF plug-flow reactor, a piece of FMOF-808-NA1 (1 cm in diameter, 0.1 cm in thickness, 3 mg) was added into a filter head as the catalytic filler. 10 mL 0.4 M N-ethylmorpholine solution containing 40 µL (250 µmol) of simulant was injected through the plug-flow reactor at a rate of 0.1 mL min^{-1} using a micropump, and the filtrate was subjected to ^{31}P NMR spectroscopic analysis every 1 mL to determine DMNP conversion. When the conversion was reduced below 100%, FMOF-808-NA1 nanozyme filter was regenerated by washing it with 50 mL water and loaded back into the plug-flow reactor.

Supporting Information

Supporting Information is available from the Wiley Online Library or from the author.

Acknowledgements

K.M. and Y.H.C. contributed equally to this work. The authors acknowledge the financial support from the Army Research Office (W911NF1910340).

© 2023 The Authors. Advanced Materials published by Wiley-VCH GmbH

Downloaded for personal academic use. All rights reserved. https://papernode.online/

This work made use of the J.B. Cohen X-ray Diffraction Facility supported by the MRSEC program of the National Science Foundation (DMR-1720139) at the Materials Research Center of Northwestern University. This work made use of Keck-II and EPIC facilities of the NUANCE Center at Northwestern University, which has received support from the Soft and Hybrid Nanotechnology Experimental (SHyNE) Resource (NSF NNCI-1542205); the MRSEC program (NSF DMR-1720139) at the Materials Research Center; the International Institute for Nanotechnology (IIN); the Keck Foundation; and the State of Illinois, through the IIN. This work made use of the IMSERC at Northwestern University, which has received support from the NSF (CHE-1048773 and DMR-0521267), the State of Illinois, and IIN. K.O.K. gratefully acknowledges support from the IIN Postdoctoral Fellowship and the Northwestern University International Institute for Nanotechnology. J.H.X. acknowledges the support from General Research Fund of the Research Grants Council of the Hong Kong SAR Government (GRF 15208420).

Conflict of Interest

O.K.F. has a financial interest in the start-up company NuMat Technologies, which is seeking to commercialize metal-organic frameworks.

Data Availability Statement

The data that support the findings of this study are available from the corresponding author upon reasonable request.

Keywords

catalytic detoxification, MOFs, nanozymes, organophosphates toxins, porous aerogels

Received: January 31, 2023
Revised: June 7, 2023
Published online: June 29, 2023

[1] R. Zhang, X. Yan, K. Fan, *Acc. Mater. Res.* **2021**, *2*, 534.
[2] L. Huang, J. Chen, L. Gan, J. Wang, S. Dong, *Sci. Adv.* **2019**, *5*, eaav5490.
[3] L. Gao, J. Zhuang, L. Nie, J. Zhang, Y. Zhang, N. Gu, T. Wang, J. Feng, D. Yang, S. Perrett, X. Yan, *Nat. Nanotechnol.* **2007**, *2*, 577.
[4] L. Gao, K. Fan, X. Yan, *Theranostics* **2017**, *7*, 3207.
[5] Q. Wang, H. Wei, Z. Zhang, E. Wang, S. Dong, *Trends Analyt. Chem.* **2018**, *105*, 218.
[6] X. Shen, Z. Wang, X. J. Gao, X. Gao, *Adv. Mater.* **2023**, doi.org/10.1002/adma.202211151.
[7] Z. W. Chen, Z. Z. Wang, J. S. Ren, X. G. Qu, *Acc. Chem. Res.* **2018**, *51*, 789.
[8] D. Duan, K. Fan, D. Zhang, S. Tan, M. Liang, Y. Liu, J. Zhang, P. Zhang, W. Liu, X. Qiu, G. P. Kobinger, G. F. Gao, X. Yan, *Biosens. Bioelectron.* **2015**, *74*, 134.
[9] T. Zhang, F. Tian, L. Long, J. L., X. Wu, *Int. J. Nanomed.* **2018**, *13*, 4795.
[10] A. Li, L. Long, F. Liu, J. Liu, X. Wu, Y. Ji, *J. Biol. Eng.* **2019**, *13*, 87.
[11] J. Han, J. Yoon, *ACS Appl. Biol. Mater.* **2020**, *3*, 7344.
[12] Y. Yang, D. Zhu, Y. Liu, B. Jiang, W. Jiang, X. Yan, K. Fan, *Nanoscale* **2020**, *12*, 13548.
[13] C. Cao, N. Yang, Y. Su, Z. Zhang, C. Wang, X. Song, P. Chen, W. Wang, X. Dong, *Adv. Mater.* **2022**, *34*, 2203236.
[14] Y. Meng, W. Li, X. Pan, G. M. Gadd, *Environ. Sci.: Nano* **2020**, *7*, 1305.
[15] C. Hong, X. Meng, J. He, K. Fan, X. Yan, *Particuology* **2022**, *71*, 90.
[16] X. Meng, D. Li, L. Chen, H. He, Q. L. Feng, J.-L. Li, G. S. Day, X.-L. Lv, H.-C. Zhou, *Chem* **2019**, *5*, 1265.
[17] S. Kitagawa, R. Kitaura, S. I. Noro, *Angew. Chem., Int. Ed.* **2004**, *43*, 2334.
[18] Z. Chen, H. Jiang, M. Li, M. OQKeeffe, M. Eddaoudi, *Chem. Rev.* **2020**, *120*, 8039.
[19] M. R. Mian, H. Chen, R. Cao, K. O. Kirlikovali, R. Q. Snurr, T. Islamoglu, O. K. Farha, *J. Am. Chem. Soc.* **2021**, *143*, 9893.
[20] J. R. Li, R. J. Kuppler, H. C. Zhou, *Chem. Soc. Rev.* **2009**, *38*, 1477.
[21] W. Fan, S. Yuan, W. Wang, L. Feng, X. Liu, X. Zhang, X. Wang, Z. Kang, F. Dai, D. Yuan, D. Sun, H. C. Zhou, *J. Am. Chem. Soc.* **2020**, *142*, 8728.
[22] L. Cao, Z. Lin, F. Peng, W. Wang, R. Huang, C. Wang, J. Yan, J. Liang, Z. Zhang, T. Zhang, L. Long, J. Sun, W. Lin, *Angew. Chem., Int. Ed.* **2016**, *55*, 4962.
[23] X. Liu, K. O. Kirlikovali, Z. Chen, K. Ma, K. B. Idrees, R. Cao, X. Zhang, T. Islamoglu, Y. Liu, O. K. Farha, *Chem. Mater.* **2021**, *33*, 1444.
[24] J. Wu, Z. Wang, X. Jin, S. Zhang, T. Li, Y. Zhang, H. Xing, Y. Yu, H. Zhang, X. Gao, H. Wei, *Adv. Mater.* **2021**, *33*, 2005024.
[25] G. Fang, R. Kang, Y. Chong, L. Wang, C. Wu, C. Ge, *Appl. Catal. B* **2023**, *320*, 121931.
[26] Y. Liu, S. Y. Moon, J. T. Hupp, O. K. Farha, *ACS Nano* **2015**, *9*, 12358.
[27] J. Wu, Y. Yu, Y. Cheng, C. Cheng, Y. Zhang, B. Jiang, X. Zhao, L. Miao, H. Wei, *Angew. Chem., Int. Ed.* **2021**, *60*, 1227.
[28] X. Huang, S. T. Zhang, Y. J. Tang, X. Y. Zhang, Y. Bai, H. Pang, *Coord. Chem. Rev.* **2021**, *449*, 214216.
[29] S. Li, Z. Zhou, Z. Tie, B. Wang, M. Ye, L. Du, R. Cui, W. Liu, C. Wan, Q. Liu, S. Zhao, Q. Wang, Y. Zhang, S. Zhang, H. Zhang, Y. Du, H. Wei, *Nat. Commun.* **2022**, *13*, 827.
[30] H. Ly, G. Fu, A. Kondinski, B. Bueken, D. Vos, T. Parac-Vogt, *J. Am. Chem. Soc.* **2018**, *140*, 6325.
[31] J. Yang, K. Li, C. Li, J. Gu, *Angew. Chem.* **2020**, *132*, 23152.
[32] P. Li, R. C. Klet, S. Y. Moon, T. C. Wang, P. Deria, A. W. Peters, B. M. Klahr, H. J. Park, S. S. Al-Juaid, J. T. Hupp, O. K. Farha, *Chem. Commun.* **2015**, *51*, 10925.
[33] L. L. Li, B. Li, D. M. Chen, J. C. Zhao, D. Q. Yang, D. H. Ma, L. Jiang, Y. P. Yang, Y. Z. Li, J. Q. Wang, *J. Biosci. Med.* **2019**, *7*, 222.
[34] M. J. Katz, J. E. Mondloch, R. K. Totten, J. K. Park, S. T. Nguyen, O. K. Farha, J. T. Hupp, *Angew. Chem., Int. Ed.* **2014**, *53*, 497.
[35] A. N. Bigley, F. M. Raushel, *Biochim. Biophys. Acta, Gen. Subj.* **2013**, *1834*, 443.
[36] J. Castro, M. C. Wasson, W. Flores, O. K. Farha, Y. Liu, *ACS Catal.* **2021**, *11*, 1424.
[37] M. S. Denny, J. C. Moreton, L. Benz, S. M. Cohen, *Nat. Rev. Mater.* **2016**, *1*, 16078.
[38] C. R. Jabbour, L. A. Parker, E. M. Hutter, B. Weckhuysen, *Nat. Chem. Rev.* **2021**, *5*, 370.
[39] G. Peterson, D. T. Lee, H. F. Barton, T. H. Epps, G. Parsons, *Nat. Rev. Mater.* **2021**, *6*, 605.
[40] K. Ma, M. C. Wasson, X. Wang, X. Zhang, K. B. Idrees, Z. Chen, Y. Wu, S. Lee, R. Cao, Y. Chen, L. Yang, F. A. Son, T. Islamoglu, G. W. Peterson, J. J. Mahle, O. K. Farha, *Chem Catal* **2021**, *1*, 721
[41] Z. Chen, K. Ma, J. J. Mahle, H. Wang, Z. H. Syed, A. Atilgan, Y. Chen, J. H. Xin, T. Islamoglu, G. W. Peterson, O. K. Farha, *J. Am. Chem. Soc.* **2019**, *141*, 20016.
[42] D. T. Lee, Z. Dai, G. W. Peterson, M. G. Hall, N. L. Pomerantz, N. Hoffman, G. N. Parsons, *Adv. Funct. Mater.* **2022**, *32*, 2108004.
[43] E. López-Maya, C. Montoro, L. M. Rodríguez-Albelo, S. D. Aznar Cervantes, A. A. Lozano-Pérez, J. L. Cenís, E. Barea, J. A. Navarro, *Angew. Chem., Int. Ed.* **2015**, *54*, 6790.
[44] B. Bueken, N. Van Velthoven, T. Willhammar, T. Stassin, I. Stassen, D. A. Keen, G. V. Baron, J. F. M. Denayer, R. Ameloot, S. Bals, D. De Vos, T. D. Bennett, *Chem. Sci.* **2017**, *8*, 3939.

© 2023 The Authors. Advanced Materials published by Wiley-VCH GmbH

Downloaded for personal academic use. All rights reserved. https://papernode.online/

[45] J. Hou, A. F. Sapnik, T. D. Bennett, *Chem. Sci.* **2020**, *11*, 310.
[46] K. Ma, T. Islamoglu, Z. Chen, P. Li, M. C. Wasson, Y. Chen, Y. Wang, G. W. Peterson, J. H. Xin, O. K. Farha, *J. Am. Chem. Soc.* **2019**, *141*, 15626.
[47] Y. H. Cheung, K. Ma, M. C. Wasson, X. Wang, K. B. Idrees, T. Islamoglu, J. Mahle, G. W. Peterson, J. H. Xin, O. K. Farha, *Angew. Chem., Int. Ed.* **2022**, *61*, e202202207.
[48] Y. H. Cheung, ; K. Ma, H. van Leeuwen, M. Wasson, X. Wang, K. Idrees, W. Gong, R. Cao, J. Mahle, T. Islamoglu, G. Peterson, M. de Koning, J. Xin, O. Farha, *J. Am. Chem. Soc.* **2021**, *143*, 16777.
[49] M. Kalaj, S. M. Cohen, *Angew. Chem., Int. Ed.* **2020**, *59*, 13984.
[50] D. T. L. Zhao, R. W. Yaga, M. G. Hall, H. F. Barton, I. R. Woodward, C. J. Oldham, H. J. Walls, G. W. Peterson, G. N. Parsons, *Angew. Chem., Int. Ed.* **2016**, *55*, 13224.
[51] M. Kalaj, M. S. Denny, K. C. Bentz, J. M. Palomba, S. M. Cohen, *Angew. Chem., Int. Ed.* **2019**, *58*, 2336.
[52] Y. Zhang, S. Yuan, X. Feng, H. Li, J. Zhou, B. Wang, *J. Am. Chem. Soc.* **2016**, *138*, 5785.
[53] J. Zhao, W. T. Nunn, P. C. Lemaire, Y. Lin, M. D. Dickey, C. J. Oldham, H. J. Walls, G. W. Peterson, M. D. Losego, G. N. Parsons, *J. Am. Chem. Soc.* **2015**, *137*, 13756.
[54] A. X. Lu, T. M. T. Ploskonka, G. W. Peterson, J. B. DeCoste, *Ind. Eng. Chem. Res.* **2017**, *56*, 14502.
[55] G. W. Peterson, A. X. Lu, H. E. Thomas, *ACS Appl. Mater. Interfaces* **2017**, *9*, 32248.
[56] K. M. Lu, K. B. Idrees, F. A. Son, R. Maldonado, M. C. Wasson, X. Zhang, X. Wang, E. Shehayeb, A. Merhi, B. R. Kaafarani, T. Islamoglu, J. H. Xin, O. K. Farha, *Chem. Mater.* **2020**, *32*, 6456.
[57] D. T. Lee, J. D. Jamir, G. W. Peterson, G. N. Parsons, *Small* **2019**, *15*, 1805133.
[58] D. T. Lee, J. D. Jamir, G. W. Peterson, G. N. Parsons, *Matter* **2020**, *2*, 404.
[59] P. Li, J. Li, X. Feng, J. Li, Y. Hao, J. Zhang, H. Wang, A. Yin, J. Zhou, X. Ma, B. Wang, *Nat. Commun.* **2019**, *10*, 2177.
[60] H. Wang, P. Rassu, X. Wang, H. Li, X. Wang, X. Wang, X. Feng, A. Yin, P. Li, X. Jin, S. L. Chen, X. Ma, B. Wang, *Angew. Chem., Int. Ed.* **2018**, *57*, 16416.
[61] D. T. Lee, J. Zhao, G. W. Peterson, G. N. Parsons, *Chem. Mater.* **2017**, *29*, 4894.
[62] Y. Chen, S. Zhang, S. Cao, S. Li, F. Chen, S. Yuan, C. Xu, J. Zhou, X. Feng, X. Ma, B. Wang, *Adv. Mater.* **2017**, *29*, 1606221.
[63] X. Ma, Y. Chai, P. Li, B. Wang, *Acc. Chem. Res.* **2019**, *52*, 1461.
[64] S. C. Li, B. C. Hu, L. M. Shang, T. Ma, C. Li, H. W. Liang, S. H. Yu, *Adv. Mater.* **2022**, *34*, 2202504.
[65] S. Y. Moon, Y. Liu, J. T. Hupp, O. K. Farha, *Angew. Chem., Int. Ed.* **2015**, *54*, 6795.
[66] J. Jiang, F. Gándara, Y.-B. Zhang, K. Na, O. M. Yaghi, W. G. Klemperer, *J. Am. Chem. Soc.* **2014**, *136*, 12844.
[67] P. Spiliopoulos, S. Spirk, T. Pääkkönen, M. Viljanen, K. Svedström, L. Pitkänen, M. Awais, E. Kontturi, *Biomacromolecules* **2021**, *22*, 1399.
[68] Eddleston, M., *Annu. Rev. Pharmacol. Toxicol.* **2019**, *59*, 341.

© 2023 The Authors. Advanced Materials published by Wiley-VCH GmbH

Downloaded for personal academic use. All rights reserved. https://papernode.online/